Folding Stability and Cooperativity of the Three Forms of 1–110 Residues Fragment of Staphylococcal Nuclease

Tao Xie, Dongsheng Liu, Yingang Feng, Lu Shan, and Jinfeng Wang
National Laboratory of Biomacromolecules, Center for Structural and Molecular Biology, Institute of Biophysics, Chinese Academy of Sciences, Beijing 100101, People's Republic of China

ABSTRACT Folding stability and cooperativity of the three forms of 1–110 residues fragment of staphylococcal nuclease (SNase110) have been studied by various biophysical and NMR methods. Samples of G-88W- and V-66W-mutant SNase110, namely G-88W110 and V-66W110, in aqueous solution and SNase110 in 2.0 M TMAO are adopted in this study. The unfolding transitions and folded conformations of the three SNase fragments were detected by far- and near-ultraviolet circular dichroism and intrinsic tryptophan fluorescence measurements. The tertiary structures and internal motions of the fragments were determined by NMR spectroscopy. Both G-88W and V-66W single mutations as well as a small organic osmolyte (Trimethylamine *N*-oxide, TMAO) can fold the fragment into a native-like conformation. However, the tertiary structures of the three fragments exhibit different degrees of folding stability and compactness. G-88W110 adopts a relatively rigid structure representing a most stable native-like β-subdomain conformation of the three fragments. V-66W110- and TMAO-stabilized SNase110 produce less compact structures having a less stable "β-barrel" structural region. The different folding status accounts for the different backbone dynamic and urea-unfolding transition features of the three fragments. The G-20I/G-29I-mutant variants of the three fragments have provided the evidence that the folding status is correlated closely to the packing of the β-strands in the β-barrel of the fragments. The native-like β-barrel structural region acts as a nonlocal nucleus for folding the fragment. The tertiary folding of the three fragments is initiated by formation of the local nucleation sites at two β-turn regions, I-18–D-21 and Y-27–Q-30, and developed by the formation of a nonlocal nucleation site at the β-barrel region. The formation of β-barrel and overall structure is concerted, but the level of cooperativity is different for the three 1–110 residues SNase fragments.

INTRODUCTION

The question ''how do proteins fold in vivo and in vitro'' has been under intensive study for several decades. It was proposed (1) that small proteins of molecular mass ~10–15 kDa fold the same way in vitro as they do in vivo. As has been well established, in vivo proteins are slowly biosynthesized on the ribosome from the N-terminus of the amino acid sequence, and there is a host of other molecular factors in the cell, such as large molecular chaperones and small chemical chaperones that play diverse supportive roles in protein folding. In vitro, the investigation of protein folding has been opened up to molecular and atomic level resolutions, centering on folding mechanisms, pathways, rates, and the driving forces of folding. Three classical hypotheses for the mechanisms of folding (2) have been proposed which put more emphasis on specific structures and pathways. The chemical physics view portrays folding as the motion of the polypeptide chain on a partially rugged, funnel-shaped energy landscape as it searches conformational space on the way to its unique native structure. On a funnel-like energy surface, proteins must pay an entropic price before the downhill tendency of the energy landscape can be manifested (3).

Staphylococcal nuclease (SNase) is composed of α- and β-subdomains and is a widely used model system for the study of protein folding. Many early studies focused on the thermodynamic and kinetic analysis of SNase folding and unfolding transitions and on the structural analysis of SNase in nonnative states. Abundant experimental data of the folding intermediates, folding stabilities, and residual structures of nonnative SNase have been accumulated. Various large SNase fragments and their mutants have been adopted for exploring the folding state and folding process of the molecule before folding to a stable structure (4–9). For the 1–102 residues SNase fragment, the G-88W and V-66W single mutation cannot drive the overall folding of the fragments G-88W102 and V-66W102, but only can make around 30–40% of the molecule to be possibly structured (4). However, the G-88V/V-66L double mutation can drive the 1–103 residues SNase fragment folding into a stable ''OB-fold'' subdomain (5). Fragment Δ131Δ, consisting of residues 1–3 and 13–140, was found in a denatured but not random coil state (6). Chemical cleavage studies of SNase fragment 1–135 and its mutants revealed a native-like state of segment 1–104 and a disordered C-terminal region (7). Investigation of 136-amino acid polypeptide of SNase (SNase136) and V-66W-mutant SNase136 (V-66W136) showed the similar conformational features which exhibited the folded β-subdomain and a disordered C-terminal region (8). Examination of the folding ability and stability of the fragments 1–140 and 1–141 indicated that both SNase fragments exhibited a native-like tertiary folding and W-140 is a key residue for the structure and stability of SNase fragments (9).

Submitted June 26, 2006, and accepted for publication November 27, 2006.

Tao Xie and Dongsheng Liu contributed equally to this work.

Address reprint requests to Jinfeng Wang, Tel.: 86-10-6488-8490(O); Fax: 86-10-6487-2026; E-mail address: jfw@sun5.ibp.ac.cn.

0006-3495/07/03/2090/18 $2.00

doi: 10.1529/biophysj.106.092155

The folding pathways of SNase with chain elongation from residue K-110 to the C-terminal region of the molecule, involving the generation of a ''β-barrel'' hydrophobic core and overall architecture of the β-subdomain, were analyzed by studying the N-terminal large fragments of SNase (10).

The 1–110 residues SNase fragment (SNase110) has a nearly complete sequence of the β-subdomain, containing a main β-barrel region and two α-helices (helices α1 and α2). In aqueous solution, SNase110 exhibits an ensemble of species containing unfolded and partially folded states (10). We found that the G-88W and V-66W single mutations and a small organic osmolyte, Trimethylamine *N*-oxide (TMAO), can drive the 110-residue SNase fragment to form a native-like folded conformation. The focus of this study was to determine the folding status and folding mechanism of G-88W110, V-66W110, and SNase110 in 2.0 M TMAO. The tertiary structures, unfolding transitions, and internal motions of the three forms of 1–110 residues SNase fragments were detected using the circular dichroism (CD), fluorescence, and heteronuclear multidimensional NMR spectroscopy for studying the folding and stability of the fragments. The results ought to contribute to a better understanding of the folding mechanism of SNase in vitro.

MATERIALS AND METHODS

Sample preparation

The SNase110 fragment containing residues 1–110 of SNase from the V8 strain of *Staphylococcus aureus* and its mutant fragments, G-88W110 and V-66W110, were expressed and purified according to the procedures described previously (11). The mutant variants [G-20I/G-29I]G-88W110, [G-20I/G-29I]V-66W110, and [G-20I/G-29I]SNase110 were produced by G-20I/G-29I double mutation of the three 110-residue SNase fragments in the corresponding expression plasmids by the QuickChange method (12). Uniformly ^{15}N- and ^{13}C-labeled fragments were obtained through bacterial growth in M9 minimal media using $^{15}NH_4Cl$ (1 g/l) and ^{13}C-glucose (2 g/l) as the sole nitrogen and carbon sources. The purity of the proteins was checked by sodium dodecylsulfate-polyacrylamide gel electrophoresis to be a single band. Samples of G-88W110, V-66W110, [G-20I/G-29I]G-88W110, and [G-20I/G-29I]V-66W110 in 90% H_2O/10% D_2O containing 1–2.0 mM proteins and 50 mM acetate buffer (pH 4.9) were prepared for NMR experiments. The samples of SNase110 and [G-20I/G-29I]SNase110 for NMR studies were prepared by dissolving 1 mM protein in 90% H_2O/10% D_2O (pH 6.0) containing 2.0 M TMAO (the purity $>$ 99.0%, purchased from Fluka, Milwaukee, WI). Samples of G-88W110, V-66W110, [G-20I/G-29I]G-88W110, [G-20I/G-29I]V-66W110, and samples of SNase110 and [G-20I/G-29I]SNase110 in 2.0 M TMAO containing 60 μM proteins and 20 mM Tris-HCl buffer (pH 7.4) were prepared for far-ultraviolet (UV) CD measurement; 120 μM G-88W110, V-66W110, [G-20I/G-29I]G-88W110, and [G-20I/G-29I]V-66W110 (pH 7.4) were used for near-UV CD measurements. Samples used for denaturation studies by CD measurements were 30 μM G-88W110, V-66W110, SNase110 in 2.0 M TMAO, and their G-20I/G-29I-double mutant variants, and those by fluorescence measurements were 6.0 μM G-88W110, V-66W110, [G-20I/G-29I]G-88W110, and [G-20I/G-29I]V-66W110 (pH 7.4) in the presence of urea at various concentrations ranging from 0 to 6.0 M with increments of 0.25 M. All the fragment samples prepared for denaturation studies were incubated overnight at 20°C before measurement. Protein concentrations were determined by UV absorption at 280 nm.

CD measurements

Far-UV CD (200–250 nm) and near-UV CD (240–300 nm) spectra of the six 110-residue SNase fragments were recorded on a Jasco (Tokyo, Japan) J-720 spectropolarimeter at room temperature. Employed were 1-mm and 10-mm cuvette pathlengths to record the far-UV and near-UV CD spectra, respectively. Five scans were averaged for each measurement. The far-UV CD spectra were used to estimate the contents of secondary structural components in the 110-residue SNase fragments by analysis of the ellipticities using programs in the software package CDPro (http://lamar.colostate.edu/~sreeram/CDPro).

Fluorescence measurements

Intrinsic fluorescence emission spectra of the 110-residue SNase fragments were measured using a Hitachi (San Jose, CA) F-4500 fluorescence spectrophotometer at 20°C. The slit width for all the measurements was 5 nm. For the intrinsic fluorescence measurements, the excitation wavelength was 295 nm for the tryptophan residue. The emission intensity of tryptophan at 325 nm was recorded for G-88W110 and V-66W110 and their G-20I/G-29I-double mutant fragments.

Determination of unfolding free energy

The unfolding process was monitored by following the changes in ellipticity and intrinsic fluorescence at wavelengths 222 and 325 nm, respectively. The unfolding free energies of G-88W110, V-66W110, and SNase110 in the presence of urea were obtained using the intensities of these signals, which were normalized to the fraction of unfolded species using the standard relation: $F_{unf} = (I - I_N)/(I_U - I_N)$, where N and U stand for the fluorescence intensity of the native and fully unfolded species (13). The F_{unf} values were calculated from the linear extrapolation of the pre- and postunfolding baselines. The unfolding free energy and m values in the relation $\Delta G = \Delta G°(H_2O) + m[D]$ were obtained from the fitting of the denaturation data to a two-state model using the standard equation (13,14) for all the six fragments, except as otherwise indicated.

NMR spectroscopy

All NMR experiments were run on a Bruker (Billerica, MA) DMX 600 spectrometer equipped with a triple-resonance cryoprobe at 305 K for G-88W110 and at 298 K for V-66W110 and SNase110 in 2.0 M TMAO. For the resonance assignments and NOE and J-coupling constant determinations, the 3D ^{1}H-^{13}C-^{15}N HNCO, HN(CA)CO, CBCA(CO)NH, HNCACB, H(CCONH), and HNHB, and the 3D ^{1}H-^{15}N total correlation spectroscopy (TOCSY)-heteronuclear single-quantum correlation (HSQC) and nuclear Overhauser effect spectroscopy (NOESY)-HSQC experiments (15,16) were performed with the samples containing 2.0 mM G-88W110, V-66W110, and with 1.0 mM SNase110 in 2.0 M TMAO. The mixing times for 3D ^{1}H-^{15}N NOESY-HSQC and TOCSY-HSQC experiments of both G-88W110 and V-66W110 were 200 ms and 80 ms, respectively. Mixing times of 150 ms and 55 ms were set for the 3D ^{1}H-^{15}N NOESY-HSQC and TOCSY-HSQC experiments of SNase110 in 2.0 M TMAO, respectively. The two-dimensional (2D) ^{1}H-^{15}N HSQC experiments were carried out with G-88W110, V-66W110, and SNase110 in 2.0 M TMAO at protein concentrations of 0.05, 0.1, 0.2, 0.5, 1.0, and 2.0 mM, and with G-20I/G-29I-mutant fragments as well. The pulsed field gradient NMR experiment for translational diffusion measurement (17) was performed with G-88W110, V-66W110, and SNase110 in aqueous solution at protein concentrations of 0.05, 0.1, 1.0, and 2.0 mM and with SNase110 in the presence of TMAO (D-9, 98%; CIL, Lawrence, MA) at protein concentrations of 0.05, 0.1, 1.0, and 2.0 mM. All data were processed and analyzed using FELIX98 (MSI/Accelrys, San Diego, CA). The data points in each indirect dimension were usually doubled by linear prediction (18) before zero filling to the appropriate size. We used 90°–60°-

shifted-square sine bell apodizations for all three dimensions before Fourier transformation. ^{1}H chemical shifts were referenced to internal 2,2-dimethyl-2-silapentane-5-sulfonate (DSS). ^{15}N and ^{13}C chemical shifts were referenced indirectly (19).

For the backbone dynamics studies, the 2D ^{15}N R_1 and R_2 HSQC and ^{1}H-^{15}N NOE experiments were performed with G-88W110, V-66W110, and SNase110 in 2.0 M TMAO at 298 K using standard methods (20). The concentration of the fragments was 1.0 mM in the relaxation experiments. The 2D ^{15}N R_2 HSQC experiment was run also with the three 110-residues SNase fragments at concentration of 0.2 mM. For ^{15}N R_1 measurements, the delay times were set to 12, 62, 142, 282, 382, 522, 822, 1202, and 1602 ms for the three fragment samples. For R_2 measurements, the relaxation delays of 8.5, 17.0, 25.4, 33.9, 50.9, 67.8, 84.8, 101.8, 118.7, 135.7, and 152.6 ms were used for the fragment samples. In the 2D ^{1}H-^{15}N NOE experiments, a delay of 2 s was followed by ^{1}H saturation for 3 s, whereas the saturation period was replaced by a delay of equivalent duration in the control experiment. Two experiments were run in an interleaved manner.

Structure calculation

Based on the sequential assignments, the NOE crosspeaks between main-chain protons and between main-chain and side-chain protons were identified for G-88W110, V-66W110, and SNase110 in 2.0 M TMAO. For calculation of three-dimensional (3D) conformations of the fragments, only the medium- and long-range NOEs were used. Dihedral angle constraints were obtained using the program TALOS (21). Restraints of $\pm 25° - \pm 60°$ were introduced for ϕ- and ψ-angles. Stereospecific assignments were obtained for G-88W110 by analysis of the HNHB spectrum, J-coupling constants, and the NOEs built between the $^{1}H_N$, $^{1}H_\alpha$, and $^{1}H_\beta$ resonances. The structure calculations were carried out on a Silicon Graphics (Mountain View, CA) station Onyx 2 employing the program CNS 1.1 (22). A family of 50 structures was generated, from which a final set of the 12 best structures was considered for use in the analysis of structural statistics.

Determination of ^{15}N relaxation parameters

Intensities for the amide ^{1}H-^{15}N crosspeaks in the 2D ^{15}N R_1, R_2, and ^{1}H-^{15}N NOE spectra were determined by measuring peak heights using FELIX software. R_1 and R_2 values for each residue were determined by fitting the measured intensities to a two-parameter single-exponential decay function. The Levenberg-Marquartt algorithm in the program GNUPLOT (ftp://ftp.dartmouth.edu/pub/gnuplot/) was used to estimate the relaxation rates and the uncertainties of the relaxation parameters. The steady-state ^{1}H-^{15}N NOEs were calculated from the ratio of peak heights in the NOE spectrum to those in the control spectrum. The root mean-square (RMS) value of the noise of background regions in the spectrum was used to estimate the standard deviation of NOE values.

The relaxation data (R_1, R_2, and ^{1}H-^{15}N NOE) were analyzed according to the model-free approach of Lipari and Szabo (23,24), using the program FAST-Modelfree 1.2 (25). Before model-free interpretation of the ^{15}N relaxation data, anisotropy in the rotational diffusion of the fragment was estimated. The rotational correlation time, τ_m, was initially estimated from R_2/R_1 ratios using the relaxation rates of a subset of residues chosen to be least affected by large amplitude fast and slow timescale motions (26). The diffusion tensor components (D_{xx}, D_{yy}, D_{zz}) were obtained by the program TENSOR 2.0 (27) to determine whether an isotropic or anisotropic diffusion model should be used in the analysis of the relaxation data. Residues with NOEs lower than 0.65 were first excluded in the above analysis. Besides, residues subject to conformational exchange were also excluded in analysis of τ_m and rotational diffusion parameters if the condition

$$(\langle T_2\rangle - T_{2,n})/\langle T_2\rangle - (\langle T_1\rangle - T_{1,n})/\langle T_1\rangle > 1.5\ \mathrm{SD} \quad (1)$$

applies, where $T_{2,n}$ and $T_{1,n}$ are the T_2 and T_1 values of residue n, and $\langle T_2\rangle$ and $\langle T_1\rangle$ are the average T_2 and T_1 values taken over residues that have not been excluded because of low NOE. SD is the standard deviation of the function calculated for these residues. The starting values of the parameters τ_m and $D_{\|}/D_{\perp}$ in the model-free analysis of the relaxation data were 8.35 ns and 1.15 for G-88W110, 9.70 ns and 1.25 for V-66W110, and 14.28 ns and 0.88 for SNase110 in 2.0 M TMAO, respectively. These calculated diffusion parameters and the R_1, R_2, and ^{1}H-^{15}N NOE relaxation data were then used as the input for the model-free analysis. The axial symmetric model-free spectral density function was chosen to derive the dynamical parameters for the three fragments. The N-H bond length was assumed to be 1.02 Å and the N-H chemical shift anisotropy was taken as -160 ppm. A Lipari-Szabo analysis (23,24) was performed for all individual residues. Five model-free parameter sets were iteratively tested and selected as described by Mandel et al. (28). A total of 500 Monte Carlo simulations were performed to estimate the errors in the model-free parameters.

RESULTS

Secondary and tertiary structures detected by CD spectra

The far-UV CD spectra in Fig. 1, *A* and *B*, were used to report the secondary structures of the 110-residue SNase fragment and its mutant variants. For comparison, the far-UV CD spectrum of full-length SNase was also presented in Fig. 1. Table 1 lists the estimated contents of secondary structural components in the 110-residue SNase fragments. The far-UV CD spectrum of G-88W110 resembles those of native SNase in Fig. 1 *A*, indicating an ordered conformation of G-88W110 having more ideal helical structures compared to the other fragments. Therefore, the apparent helix content of G-88W110 is higher than the other fragments (Table 1). SNase110 in aqueous solution provided a pronounced negative signal at ~204 nm and a broad shoulder at ~222 nm in the far-UV CD spectrum, which indicated a conformation exhibiting a transient equilibrium involving species containing partially folded and unfolded states (Fig. 1 *A*). However, 2.0 M TMAO facilitated SNase110 to produce a unique far-UV CD spectrum, which seems to be an additive result of the relatively high β-strand and low α-helix contents of the fragment. V-66W110 showed a negative signal at ~207 nm and a broad shoulder at 222 nm in the far-UV CD spectrum (Fig. 1 *A*). This reflected a folded conformation having less ordered secondary structures in V-66W110 as compared with the far-UV CD spectra of G-88W110 and SNase110 in aqueous solution. The diminished intensity in the ellipticity at 222 nm in the far-UV spectrum of V-66W110 indicated much less α-helix content of V-66W110 than those of G-88W110, since the far-UV CD signal is sensitive to the secondary structure and, particularly, to the α-helix content of a polypeptide.

The near-UV CD spectrum is dominated by tryptophan ellipticity and thus is used as an indication of tertiary structure around the tryptophan residue in 110-residue SNase mutant variants. In the near-UV region, native SNase showed a pronounced negative signal at 277 nm, which can be considered an index of the uniqueness of SNase tertiary structure (Fig. 1 *C*). The explicit negative CD signal of G-88W110 at ~277 nm in the near-UV region provided an indication of substantial tertiary structure of this fragment. V-66W110,

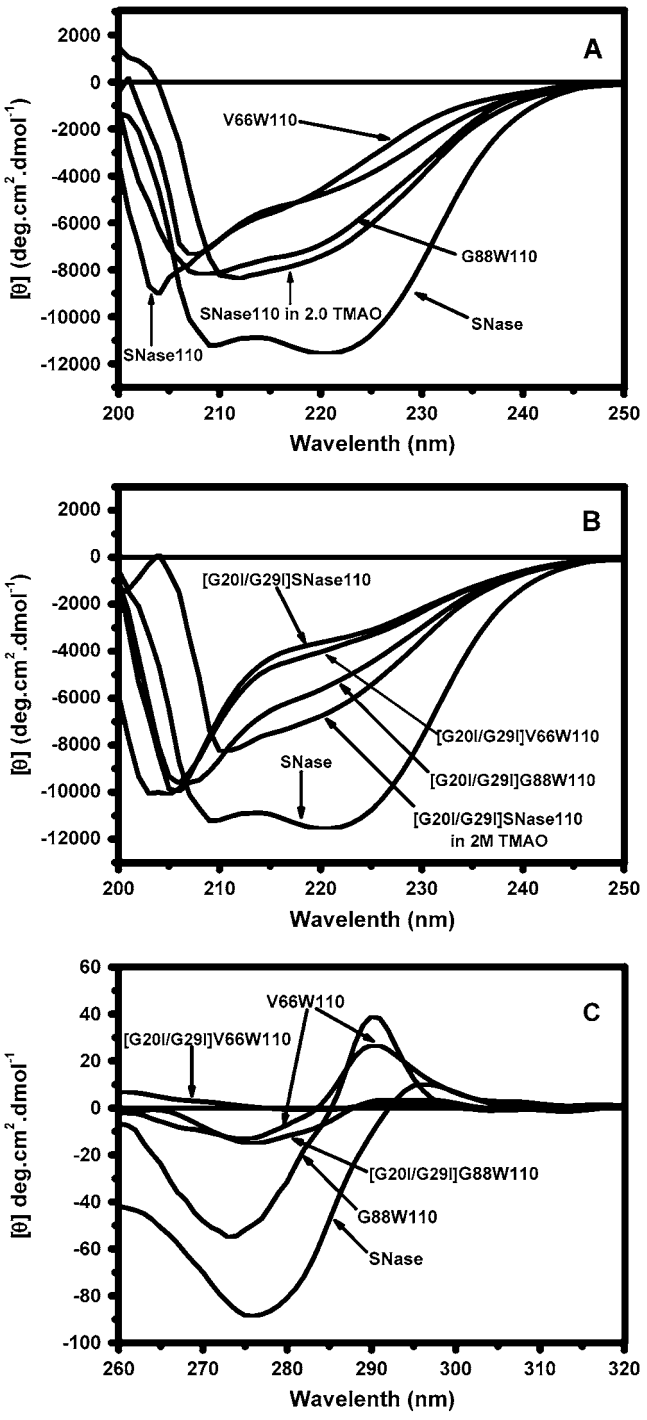

FIGURE 1 CD spectra measured for G-88W110, V-66W110, SNase110, and SNase110 in 2.0 M TMAO (*A*) and their G-20I/G-29I-double mutant variants (*B*) in far-UV region, and for G-88W110, V-66W110, [G-20I/G-29I]G-88W110, and [G-20I/G-29I]V-66W110 in near-UV region (*C*). For comparison, the far-UV and near-UV CD spectra of native SNase are provided.

showing a noticeable CD signal at ~277 nm in the near-UV region, exhibited a certain degree of tertiary folding in its conformation. Conformations of the three fragments probably can be broken down by G-20I/G-29I double mutation

TABLE 1 Secondary structure contents estimated for three 110-residue SNase fragments and their mutant variants

	α-Helix	β-Sheet	β-Turn	Loop or coil
Full-length SNase				
SNase149 (NMR-native structure)*	0.248	0.228	0.081	0.449
SNase149 (CD)†	0.328	0.162	0.197	0.319
Variant 1–110 residues SNase fragment‡				
G-88W110	0.192	0.284	0.191	0.326
V-66W110	0.121	0.334	0.206	0.323
SNase110 (2.0 M TMAO)	0.122	0.319	0.235	0.325
[G-20I/G-29I]G-88W110	0.165	0.273	0.183	0.371
[G-20I/G-29I]V-66W110	0.137	0.252	0.194	0.398
[G-20I/G-29I]SNase110 (2.0 M TMAO)	0.071	0.276	0.254	0.399
SNase110	0.110	0.265	0.167	0.448
SNase110 (NMR-native structure)§	0.200	0.200	0.109	0.381

*The estimated secondary structure content of native SNase(V8) based on the actual coordinates.

†The estimated secondary structure content of full-length SNase obtained by analysis of its far-UV CD spectrum using programs in the software package CDPro.

‡The estimated secondary structure content of 110-residue SNase fragments obtained by analysis of their far-UV CD spectra using programs in the software package CDPro.

§The estimated secondary structure content of SNase110 assuming all native structural elements from full-length protein were stable in the 110-residue SNase fragment. The secondary structural elements of 1–110 residues segment of full-length SNase(V8) were adopted in the estimation.

(Fig. 1 *B*). The far-UV CD spectra indicated the increase of disordered components in the conformations of G-20I/G-29I-double mutant variants of 110-residue SNase fragments (Fig. 1 *B* and Table 1). The random coil features dominating over the conformation of [G-20I/G-29I]V-66W110 were delineated by the pronounced negative peak at ~204 nm and the vanished negative signal at 277 nm in the far- and near-UV CD spectra, respectively, of the fragment. Apparently, no ordered tertiary structure was formed in [G-20I/G-29I] V-66W110. The unstructured features in the far-UV CD spectrum and the very weak signal in the near-UV region of [G-20I/G-29I]G-88W110 (Fig. 1, *B* and *C*) revealed a partially folded component in the conformation of G-20I/G-29I double mutant G-88W110.

Urea unfolding transitions of the fragments

The unfolding transitions of G-88W110, V-66W110, and SNase110 in 2.0 M TMAO and their G-20I/G-29I-mutant variants were detected using the far-UV CD and intrinsic tryptophan fluorescence measurements. The CD spectra of G-88W110, V-66W110, and SNase110 in 2.0 M TMAO upon unfolding measured after 40-fold dilution of the unfolded fragments in 6.0 M urea showed full restoration, indicating full reversibility of the unfolding transition (Fig. 1 in Supplementary Materials). The apparent free energy for unfolding in the presence of urea ($\Delta G°(H_2O)$) and the slope of the transition (m) were then calculated by fitting unfolding curves using a two-state mechanism model (13,14). Table 2

TABLE 2 Thermodynamic parameters obtained for urea-induced unfolding of G-88W110, V-66W110, and SNase110 in 2.0 M TMAO

	CD at 222 nm*		Fluorescence at 325 nm†	
110-residue SNase fragments	$\Delta G°(H_2O)$ kcal/mol	m kcal/(M·mol)	$\Delta G°(H_2O)$ kcal/mol	m kcal/(M·mol)
G-88W110	3.54 ± 0.25	−1.45 ± 0.09	3.59 ± 0.55	−1.53 ± 0.21
V-66W110	1.57 ± 0.08‡	−0.78 ± 0.04‡	1.11 ± 0.32	−1.29 ± 0.09
SNase110 (2.0 M TMAO)	2.23 ± 0.10‡	−0.68 ± 0.04‡		
Full-length SNase§	5.72 ± 0.23	−1.95 ± 0.08	5.79 ± 0.26	−1.93 ± 0.08

*Estimated average error from three repeated experiments for the three fragments in $\Delta G°(H_2O)$ is $< \pm 0.2$ kcal/mol and in m is $< \pm 0.10$ kcal/(M·mol).
†Estimated average error from three repeated experiments in $\Delta G°(H_2O)$ is $< \pm 0.3$ kcal/mol and in m is $< \pm 0.15$ kcal/(M·mol).
‡Fitting done by fixed m_n and I_u values taken from urea-induced denaturation.
§For comparison, the estimated thermodynamic parameters for urea-induced unfolding of native SNase are provided.

lists the estimated values of $\Delta G°(H_2O)$ and m for these fragments. The unfolding profiles (Fig. 2) were different for the three fragments having different degrees of tertiary folding in native state as suggested by CD measurements. The nonsigmoidal unfolding transitions of [G-20I/G-29I] G-88W110, [G-20I/G-29I]V-66W110, and [G-20I/G-29I] SNase110 in 2.0 M TMAO (Fig. 2 in Supplementary Materials) indicated disruption of the tertiary folding of the three fragments by G-20I/G-29I double mutation.

Fig. 2 also shows the urea-induced unfolding transition of full-length SNase as monitored by CD and fluorescence spectroscopy. Unfolding of native SNase exhibited a two-state process. Both CD and fluorescence signals showed the same transition, having a single and sharp sigmoidal changes (Fig. 2 *A*). The unfolding of G-88W110 was followed with CD and fluorescence. The sigmoidal changes of CD and fluorescence signals of G-88W110 were nearly superimposable (Fig. 2 *B*). However, the discrepancies between CD and fluorescence results were observed for V-66W110 (Fig. 2 *C*). This may correlate with the tertiary folded conformation of V-66W110. The unfolding curve from CD measurement is associated with the less ordered α-helix structure in V-66W110. Nevertheless, the unfolding curve of V-66W110 from fluorescence measurement indicates the tertiary conformation of β-barrel in the local environment of W-66, since the intrinsic tryptophan fluorescence signal is a sensitive criterion for tertiary structure around the tryptophan residue in protein. The unfolding transition of SNase110 in 2.0 M TMAO was followed by CD only, because there is no tryptophan residue contained in this fragment. Compared to native SNase and G-88W110, SNase110 in 2.0 M TMAO unfolded with a single but shallow transition (Fig. 2 *C*).

The equilibrium behaviors of the three 110-residue SNase fragments in the urea-induced unfolding process are quite different. As is indicated in Table 2, G-88W110 has relatively high unfolding free energy among the fragments. The m-values for G-88W110 estimated from CD and fluorescence measurements are nearly the same. At 2.0 M TMAO, the unfolding free energy of SNase110 is similar to those of G-88W110, but the m-value is lower than those of G-88W110. V-66W110 has the lowest unfolding free energy of the three 110-residue SNase fragments. However, the estimated m-values for V-66W110 from CD and fluorescence are close to SNase110 in 2.0 M TMAO and G-88W110, respectively.

Secondary chemical shifts

Fig. 3 shows the 2D ^{1}H-^{15}N HSQC spectra of the three 110-residue SNase fragments. The spectra of G-88W110, V-66W110, and SNase110 in 2.0 M TMAO showed well-dispersed crosspeaks (Fig. 3, *A–C*). However, [G-20I/G-29I] V-66W110 and [G-20I/G-29I]SNase110 in 2.0 M TMAO provided the spectra with unstructured and aggregated features, respectively (Fig. 3 in Supplementary Materials). The spectrum of [G-20I/G-29I]G-88W110 (Fig. 3 *D*) is similar to those of SNase110 in aqueous solution (10). Sequential backbone assignments were determined for G-88W110, V-66W110, and SNase110 in 2.0 M TMAO using a series of 3D ^{1}H-^{13}C-^{15}N triple-resonance NMR experiments. Respectively, 100%, 86%, and 93% backbone resonances of G-88W110 (10), V-66W110, and SNase110 in 2.0 M TMAO were assigned. Most of the backbone resonances for helix α2 and a few for helix α1 of V-66W110 could not be assigned. This is consistent with the CD observations that V-66W110 has much less α-helix content compared to the other two fragments. The assigned ^{15}N and ^1H_N resonances of V-66W110 and SNase110 in 2.0 M TMAO are indicated in Fig. 3.

Secondary chemical shifts (29) of $^1H_\alpha$ resonances (δH_α) of G-88W110 (10), V-66W110, and SNase110 in 2.0 M TMAO are presented in Fig. 4 *A*. The secondary structural elements of native protein, SNase of V8 strain (SNase(V8)) (15,16), are indicated in Fig. 4 *B*. For comparison, the secondary chemical shifts (δH_α) of SNase(V8) are also shown in Fig. 4 *A*. The δH_α of the three fragments was compared to those of SNase(V8) and the differences in δH_α (ΔH_α) are given in Fig. 4 *A*. The δH_α values of G-88W110, V-66W110, and SNase110 in 2.0 M TMAO are very similar to those of SNase(V8), except the residues in the sequence region L-36–E-57 and pdTp-binding loop (p-loop, D-77–L-89) as well as in the C-terminal of the fragments (Fig. 4). This indicates the tendencies toward the formation of native-like secondary structures in the three fragments. Residues V-39-D-40-T-41 and A-109-K-110-V-111 form a short two-strand antiparallel β-sheet (β_{III}) in SNase(V8) (30). Therefore, truncating the C-terminal portion of

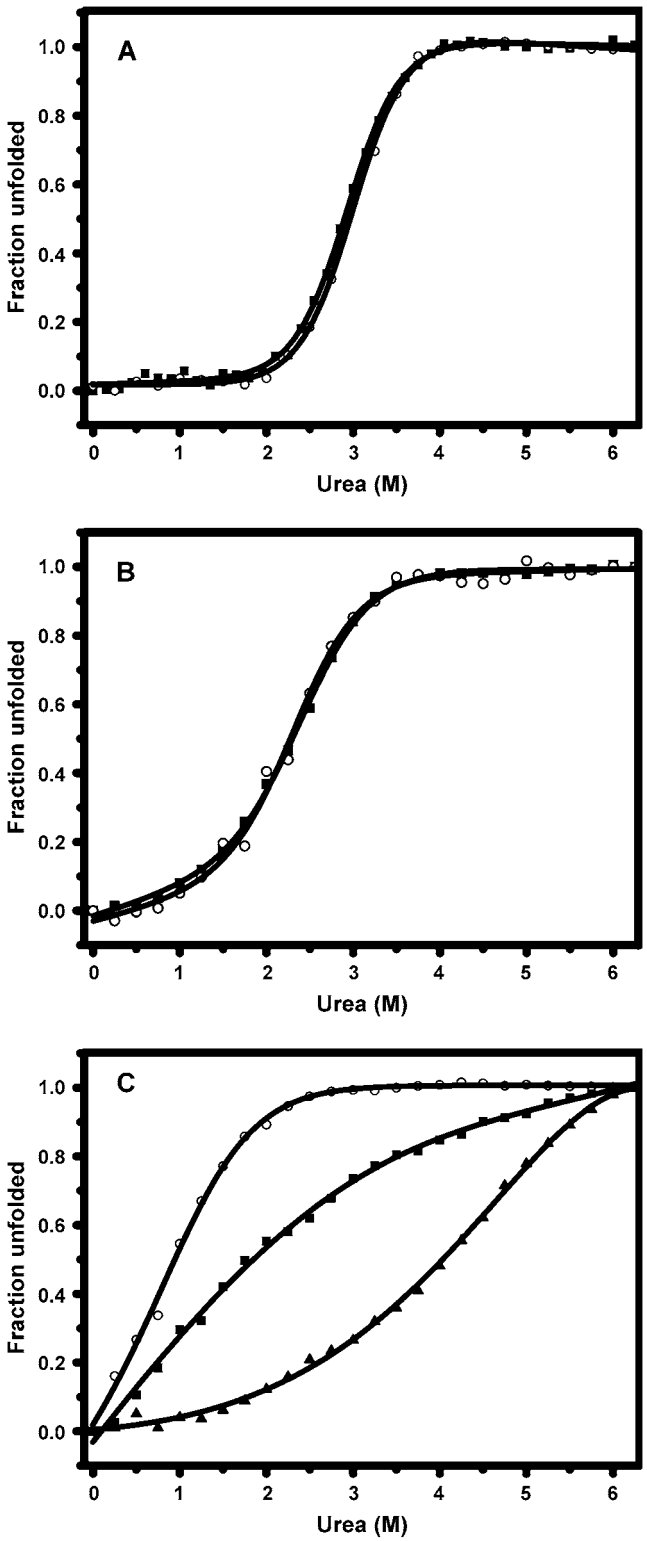

FIGURE 2 Urea-induced unfolding transitions monitored by far-UV CD at 222 nm (■) and intrinsic fluorescence at 325 nm (○) for full-length SNase (*A*), G-88W110 (*B*), and V-66W110 (*C*). (*C*) (▲) The unfolding transition of SNase110 in 2.0 M TMAO monitored by far-UV CD. The fitting of experimental data (*continuous line*) was accomplished according to the two-state mechanism model.

the enzyme sequence at K-110 greatly perturbed the secondary chemical shifts of L-38–D-40 in the fragments (Fig. 4 *A*). Segment P-42–E-57 was identified as a ω-loop in the native enzyme molecule (30). δH_α of residues K-53, Y-54, and G-55 in the segment P-42–E-57 of the three fragments are different from those of SNase(V8). Considering the changes in δH_α for residues L-38–D-40, it seems that the sequence region P-42–E-57 is not a ω-loop in the fragments (Fig. 4 *A*) and the segment L-36–E-57 appears as a disordered loop linking strand $\beta 3$ and helix $\alpha 1$ (we shall call the region L-36–E-57 as $L_{\beta 3\alpha 1}$ hereafter). The explicit changes in δH_α of corresponding residues in p-loop of the fragments, especially the large ΔH_α for T-82 of V-66W110 and G-88W110, G-88 of V-66W110, and L-89 of SNase110 in 2.0 M TMAO (Fig. 4 *A*), reveal that the p-loop of the fragments differs from that of SNase(V8) in conformation. Overall, the δH_α and ΔH_α values indicate the native-like conformations of G-88W110, V-66W110, and SNase110 in 2.0 M TMAO and the differences in backbone conformations of p-loop and the loop $L_{\beta 3\alpha 1}$ of the three fragments.

Tertiary NOE contacts

The NOE assignments were obtained for G-88W110, V-66W110, and SNase110 in 2.0 M TMAO (Fig. 4 in Supplementary Materials). Only the NOEs between main-chain protons and between main-chain and side-chain protons were identified. The assigned medium-range and long-range NOEs for G-88W110 were more than those for full-length SNase(V8) (30). However, only 27% and 54% NOEs of SNase(V8) were identified for V-66W110 and SNase110 in 2.0 M TMAO, respectively, due to the incomplete resonance assignments. The tertiary NOE contacts of the three fragments are illustrated in the NOE contact maps (Fig. 5), which are similar to those of native SNase (30) (Fig. 5 in Supplementary Materials). In Fig. 5, the medium- and long-range NOEs between main-chain protons and between main-chain and side-chain protons within the β-barrel and α-helix regions of the fragments are indicated above the diagonal. Below the diagonal, the NOE contact maps show the medium- and long-range ^1H-^1H NOEs between the secondary structural elements of the fragments. Most NOEs identified for G-88W110, V-66W110, and for SNase110 in 2.0 M TMAO are similar. In the region above the diagonal of Fig. 5, all three fragments show a great quantity of NOEs between residues in the β_I-pleated sheet consisting of strands $\beta 1$, $\beta 2$, and $\beta 3$, and the β_{II}-pleated sheet consisting of strands $\beta 4$, $\beta 5$, and $\beta 6$ (Fig. 4 *B*). There is an exception that SNase110 in 2.0 M TMAO lacks the ^1H-^1H NOEs between strands $\beta 2$ and $\beta 5$, and between $\beta 3$ and $\beta 6$, which can be observed for G-88W110 and V-66W110. This implies that the β_I- and β_{II}-pleated sheets are more flexible in SNase110 in 2.0 M TMAO. The α-helices ($\alpha 1$ and $\alpha 2$) of G-88W110 and SNase110 in 2.0 M TMAO showed a large number of interresidue NOEs. However, only the C-terminal portion of helix $\alpha 1$ in V-66W110 provided a number of

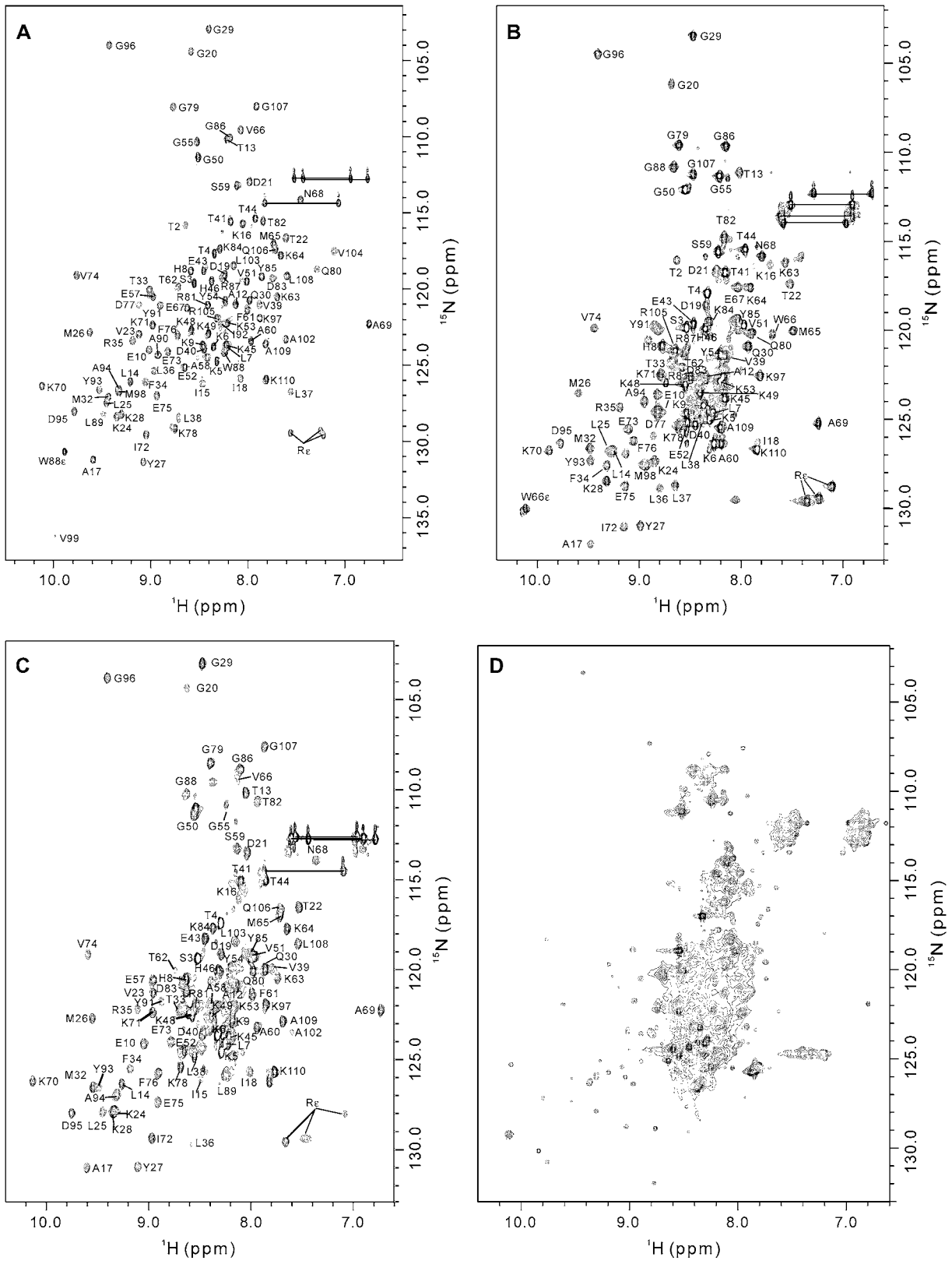

FIGURE 3 2D ^{1}H-^{15}N HSQC spectra of fragments: G-88W110 (*A*), V-66W110 (*B*), SNase110 in 2.0 M TMAO (*C*), and [G-20I/G-29I]G-88W110 (D). NMR resonance assignments were given by the one-letter amino acid code and the sequence positions.

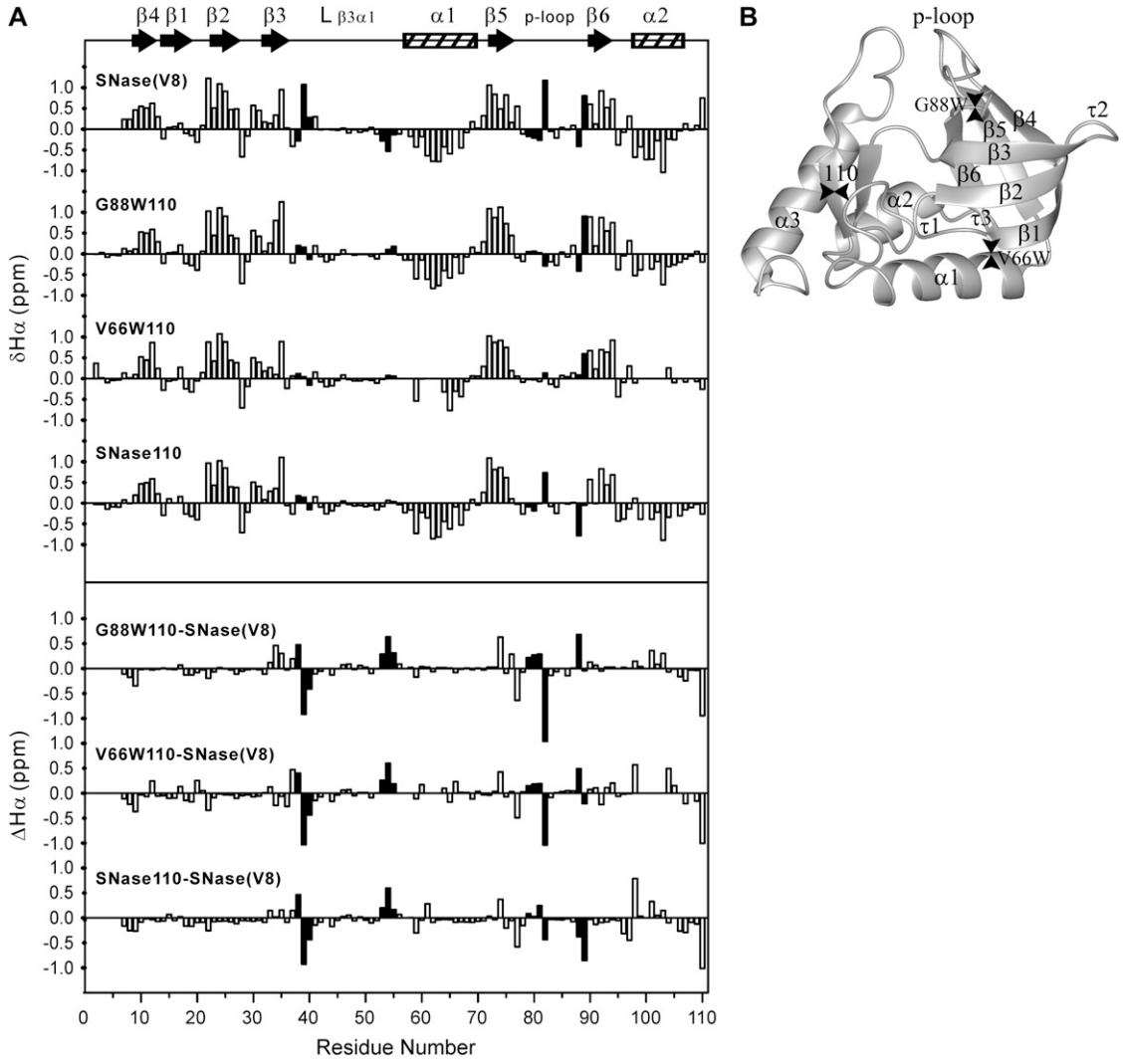

FIGURE 4 (*A*) Histograms of the secondary chemical shifts for $^1H_\alpha$ resonances (δH_α) of G-88W110[10], V-66W110, and SNase110 in 2.0 M TMAO and the differences in δH_α of the three fragments from those of native SNase(V8) (ΔH_α). The secondary structures of the fragments are labeled at the top of the figure. (*B*) Ribbon representation of the native SNase structure. The regular secondary structural elements (three α-helices: α1, 57–69; α2, 98–106; α3, 122–126; six β-strands: β1, 13–17; β2, 22–26; β3, 31–35; β4, 8–11; β5, 72–76; β6, 90–93; and three β-turns: τ1, 18–21; τ2, 27–30; τ3, 94–97) are indicated. Arrows indicate the truncation and mutation sites.

NOEs. Below the diagonal of the NOE contact maps, the NOEs between residues in the N-terminal of p-loop and strand β4, C-terminal of p-loop and strand β3, helix α1 and strands β1 and β2, $L_{\alpha1\beta5}$ (loop linking α1 and β5), and $L_{\alpha2\beta6}$ (loop linking α2 and β6), are common for all the fragments. This indicates the similarity between the three fragments in spatial arrangement of the p-loop and helices relative to β-pleated sheets. The NOEs generated by residues in helix α1 with those in helix α2 can be observed for G-88W110 and SNase110 in 2.0 M TMAO, but not for V-66W110. G-88W110 is the only fragment providing the NOEs between L-36 and residues in segment D-21–V-23. The above described NOEs depict the tertiary NOE contacts between secondary structural elements of the three fragments. The three SNase fragments show very similar spatial arrangements of secondary structures. The differences in NOE contacts of the three fragments may correlate with the different folding status of the fragments.

3D solution structures

The 3D solution structure of G-88W110 was well determined based on the assigned NOEs. The NOE contact maps of V-66W110 and SNase110 in 2.0 M TMAO are very similar to those of G-88W110 although they lack a number of NOEs. Therefore, the tertiary structures of V-66W110 and SNase110 in 2.0 M TMAO were also calculated for a better understanding of the folding properties of the 110-residue SNase fragment. For each of the three fragments, the final ensemble of 12 structures was converged with relatively low

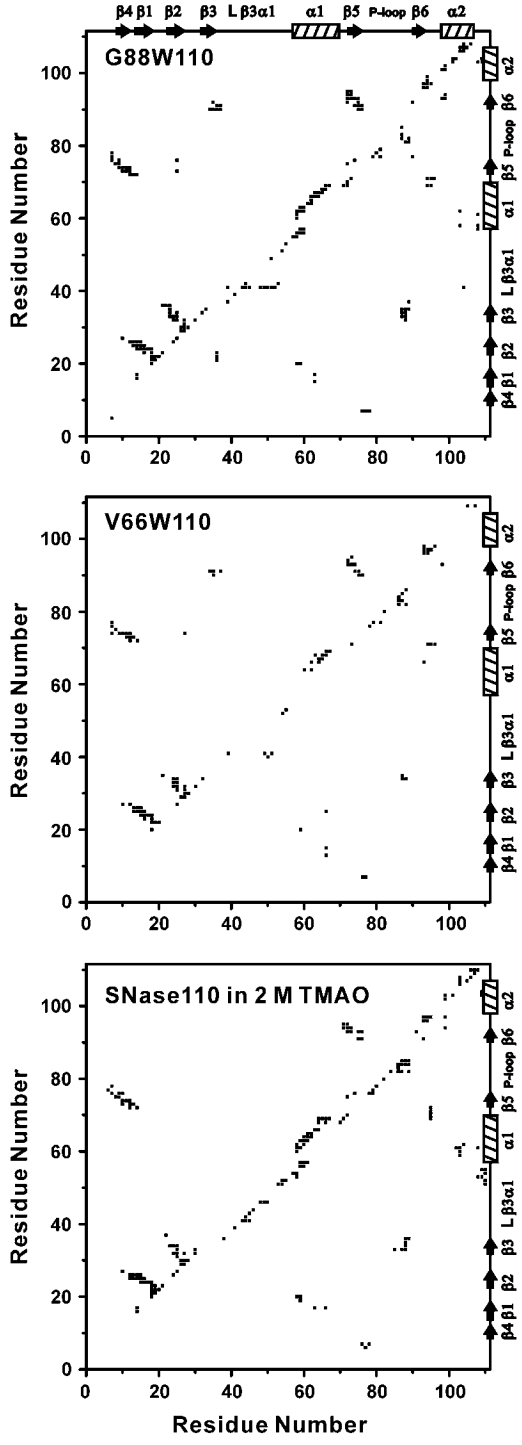

FIGURE 5 NOE contact maps of G-88W110, V-66W110, and SNase110 in 2.0 M TMAO. Only the medium- and long-range NOEs are marked in the map. The secondary structures of the fragments are labeled at the top and side of the figure. NOEs within the β-barrel and α-helix are given above the diagonal, and those between them are given below.

backbone RMS deviations and low target function energy compared to the rest of the calculated structures in each case. Structural statistics for structures of the three fragments are given in Table 3. The stereochemical quality of the backbone coordinates of each structural family was analyzed using the program PROCHECK_NMR (31). The results of the Ramanchandran map analysis are given in Table 3. Best-fit superpositions of the backbone heavy atom coordinates of the 12 structures for G-88W110, SNase110 in 2.0 M TMAO, and V-66W110 by MOLMOL (32) are shown in Fig. 6. The obtained ensemble of solution structures for G-88W110 is the best of the three fragments.

The calculated solution structures for all three fragments are similar to the corresponding part of the 3D solution structure of SNase(V8) (30) (Fig. 6), which is regarded as a β-subdomain of SNase. However, differences in conformations are observed between fragments and native SNase. The segment L-36–P-42, containing a regular β-strand V-39–T-41 (β7) in native SNase(V8), shows a different conformation in G-88W110. Residues T-41 and D-21 are involved in formation of a coordinate site for Ca^{2+} association, and $^{13}C_\alpha$ of D-21 is ~6.2 Å distant from $^{13}C_\alpha$ of T-41 in SNase(V8). However, the averaged distance between $^{13}C_\alpha$ of T-41 and D-21 is ~12.7 Å in the structures of G-88W110. Residue D-21 is located in a well-formed β-turn of β-barrel. Therefore, the backbone conformation of segment L-36–P-42 in G-88W110 is quite unlike those of SNase(V8). In the structure of SNase(V8), the p-loop linking strands β5 and β6 twisted with respect to the spatial arrangement of strands β5 and β6, the N-terminal half segment of the loop linking strand β5 leans toward the left side, and the C-terminal half segment of the loop which connects to strand β6 leans toward the right side (Fig. 4 *B*). The averaged distance between $^{13}C_\alpha$ of the terminal residues (D-77 and L-89) of p-loop is ~7.4 Å for G-88W110, whereas it is ~7.9 Å for SNase(V8). Apparently, the conformation of the p-loop in G-88W110 is similar to that of SNase(V8). Therefore, the tertiary folding of G-88W110 produces an ordered conformation representing a very native-like β-subdomain. However, the NMR-derived structures of SNase110 in 2.0 M TMAO and V-66W110 are less precise, although they adopt native-like tertiary conformations. The helix structures in V-66W110 and SNase110 in 2.0 M TMAO are poorly determined, especially the helix α2 in V-66W110, due to the lower percentage of the identified NOE crosspeaks. A disordered loop $L_{\beta3\alpha1}$ links up the strand β3 and helix α1 in the tertiary folding of all three fragments.

Apparent molecular size

To assess whether G-88W110, V-66W110, and SNase110 aggregate under the experimental conditions, the apparent molecular sizes of the three fragments were measured at various protein concentrations. The translational diffusion coefficient is commonly used to determine the apparent radius of a molecule under study. The relationship between diffusion coefficient D and solvated particle radius R is expressed by the Stokes-Einstein equation:

$$D = KT/(6\pi\eta R) \quad (2)$$

TABLE 3 Distance and dihedral angle restraints used for the structure calculations and structural statistics for the families of 12 structures of G-88W110, V-66W110, and SNase110 in 2.0 M TMAO

Constraints	G-88W110	SNase110 (2M TMAO)	V-66W110
Number of distance restraints			
Total NOEs	702	362	191
Intraresidual NOEs	0	0	0
Sequential ($\|i-j\|=1$)	0	0	0
Medium range ($\|i-j\|<5$)	263	196	71
Long range ($\|i-j\|\geq 5$)	439	166	120
Dihedral angle restraints			
ϕ -angle	82	82	84
ψ -angle	87	79	79
CNS energies (kcal/mol):			
E_{total}	189.55 ± 22.95	104.35 ± 13.74	100.20 ± 35.90
E_{Bond}	7.46 ± 1.18	3.35 ± 0.63	2.88 ± 1.30
E_{Angle}	84.87 ± 10.36	55.08 ± 3.94	55.75 ± 10.48
E_{Improp}	11.14 ± 3.05	4.14 ± 1.28	6.04 ± 3.71
E_{Vdw}	68.34 ± 8.89	35.13 ± 6.62	24.77 ± 9.50
E_{NOE}	16.32 ± 4.57	5.36 ± 2.29	4.76 ± 4.40
PROCHECK_NMR Ramachandran map analysis			
Most favored regions	64.4%	64.9%	64.5%
Additional allowed regions	29.2%	27.7%	31.6%
Generously allowed regions	4.4%	4.9%	2.4%
Disallowed regions	2.0%	2.6%	1.4%
RMS deviations of backbone C′, N, and C_α (Å)			
$\langle SA\rangle_\beta$ versus $\langle SA\rangle_\beta$	0.45	0.77	1.01
$\langle SA\rangle_{\alpha\beta}$ versus $\langle SA\rangle_{\alpha\beta}$	0.48	0.99	1.34
$\langle SA\rangle_{\text{all}}$ versus $\langle SA\rangle_{\text{all}}$	2.24	2.41	7.28

$\langle SA\rangle$: Ensemble of the 12 structures; $\langle SA\rangle$: mean structure. ''β'', ''$\alpha\beta$'', and ''all'' denote the residues in β regions, α and β regions, and whole structure, respectively.

where K is the Boltzmann constant, T is the absolute temperature, and η is the fluid viscosity. The diffusion coefficients of the 110-residue SNase fragments were obtained by translational diffusion measurements. For determining the apparent molecular radius of G-88W110 and V-66W110 in aqueous solution and SNase110 in 2.0 M TMAO, the diffusion coefficient ratio of the reference molecule dioxane to each fragment in aqueous solution or in the presence of TMAO was calculated. To convert the diffusion coefficient ratios of the three fragments to the apparent molecular radius, R, for each fragment, the diffusion coefficient ratio of dioxane to full-length SNase (149 a. a.), which has a known radius of 16.2 Å (33), was obtained under the same experimental conditions.

Variation of the calculated diffusion coefficient ratio and apparent molecular radius for the three SNase fragments at different protein concentrations are shown in Fig. 7. Approximately the same molecular radii were obtained for each of G-88W110 and V-66W110 in aqueous solution and SNase110 in the presence of TMAO at different protein concentrations. However, the concentration dependence of molecular size of SNase110 in aqueous solution was observed (Fig. 7), indicating the aggregation of SNase110 in aqueous solution at high concentration. This implies that G-88W110 and V-66W110 in aqueous solution and SNase110 in 2.0 M TMAO show no complex aggregate under study. The monomeric states of G-88W110, V-66W110, and SNase110 in 2.0 M TMAO were confirmed further by the 2D ^{1}H-^{15}N experiments performed with the fragments at concentrations of 0.05–2.0 mM. The chemical shifts and line widths of crosspeaks in the 2D ^{1}H-^{15}N HSQC spectra of 2.0-mM SNase fragments are very close to those of 0.05-mM fragments. (Fig. 6 in Supplementary Materials). Therefore, no aggregation occurs to each of the three fragments under the experimental conditions.

Fig. 7 indicates that the apparent molecular radius of G-88W110 is smaller than those of native SNase. However, the apparent molecular radius of V-66W110 has a value approximate to the value obtained for native SNase. For SNase110 in 2.0 M TMAO, a molecular size larger than those of full-length SNase is obtained. The differences in the apparent molecular radii are supposed to correlate with the different compactness in folding G-88W110, V-66W110, and SNase110 in 2.0 M TMAO, since they have a similar native-like β-subdomain structure. The molecular radius can be used as an index of the degree of compactness of the three 110-residue SNase fragments in this study.

Backbone dynamics

The T_1 and T_2 relaxation properties of G-88W110, V-66W110, and SNase110 in 2.0 M TMAO at 298 K are quite different (Fig. 8). However, such a large difference in

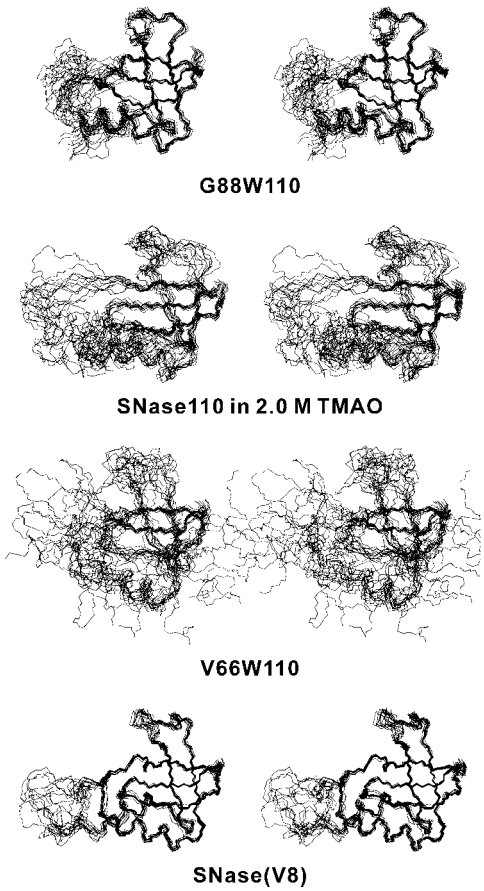

FIGURE 6 Superposition of the 12 conformers of G-88W110, V-66W110, and SNase110 in 2.0 M TMAO, and native SNase(V8) obtained using MOLMOL. The N-terminal seven residues of all structures and the sequence region V-111–Q149 of SNase(V8) are not shown.

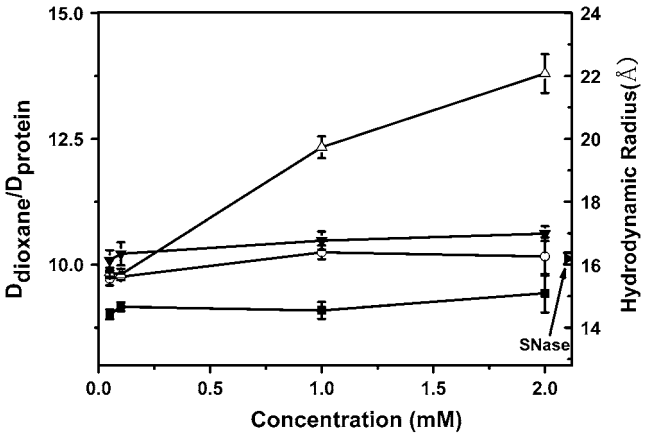

FIGURE 7 Translational diffusion coefficients and apparent molecular radii obtained for G-88W110 (■), V-66W110 (○), and SNase110 in aqueous solution (Δ) and for SNase110 in 2.0 M TMAO (▼) at different protein concentrations.

R_1 and R_2 rates between the three 110-residue SNase fragments is not caused by aggregation of the fragments, but reflects the intrinsic relaxation properties of each fragment. The independence of molecular sizes of the three fragments on protein concentrations and the comparable R_2 values for each fragment at a concentration of 1.0 mM with those of 0.2 mM (Fig. 7 in Supplementary Materials) insured that the concern for aggregation effect can be excluded in the interpretation of relaxation data.

The relaxation data were analyzed for individual residues of the fragments by the Liparli-Szabo approach (23,24). The determined correlation times for overall rotational motion (τ_m) of the fragments are 8.20 ± 0.03, 9.75 ± 0.05, and 14.20 ± 0.07 ns, respectively, for G-88W110, V-66W10, and SNase110 in 2.0 M TMAO. The different τ_m values for the three 110-residue fragments may be due to their different degree of compactness. The less compact structure of V-66W110 may hinder the fragment from more freely molecular tumbling in aqueous solution. For TMAO-stabilized SNase110, having a lower degree of compactness compared to G-88W110, the presence of 2.0 M TMAO increases the viscosity of the sample solution, hence reducing significantly the molecular tumbling of this fragment. The compact structure of G-88W110 makes the tumbling of the fragment faster than the other two fragments.

The general order parameter, S^2, and effective correlation time, τ_e, which describe the fast internal reorientation motions of the N-H bond vector were obtained for the fragments. The plot of the generalized order parameter, S^2, and internal correlation time, τ_e, against residue number for the three fragments are given in Fig. 8. A large number of residues in the disordered loop $L_{\beta3\alpha1}$ and in both N- and C-terminal regions (A1–K9 and L108–K-110) of all the three fragments have S^2 values well below 0.7 and τ_e values higher than 0.4 ns, indicating higher internal mobility and flexibility of these regions. The average S^2 value was calculated for all three fragments by averaging over most residues in secondary structural elements: α-helix, β-strand, and pdTp-binding loop, excluding the residues in the regions with large amplitude fast internal motions, namely the disordered $L_{\beta3\alpha1}$ loop and both terminal regions in the fragments. For the vast majority of the residues in the secondary structural regions of G-88W110, the S^2 values of backbone amide groups spread in a range from 0.87 ± 0.03 to 0.99 ± 0.03 with an average S^2 value of 0.93 ± 0.04. These data suggest a relatively rigid structure for most of the G-88W110 with the exception of the loop $L_{\beta3\alpha1}$. The larger spread order parameters with a lower average S^2 value (0.85 ± 0.13) were obtained for V-66W110 as compared with G-88W110. Residues in the β-barrel region have the S^2 values spread from 0.78 ± 0.07 to 0.99 ± 0.02, and residues in the p-loop at sequence positions: 79, 80, 81, 83, 85, 86, 87, and 88 of V-66W110 display S^2 values < 0.7 and τ_e values > 1.2 ns, which indicates that V-66W110 has a highly flexible p-loop with very low motional restriction. The backbone amide groups in disordered loop $L_{\beta3\alpha1}$ of V-66W110 show largely reduced

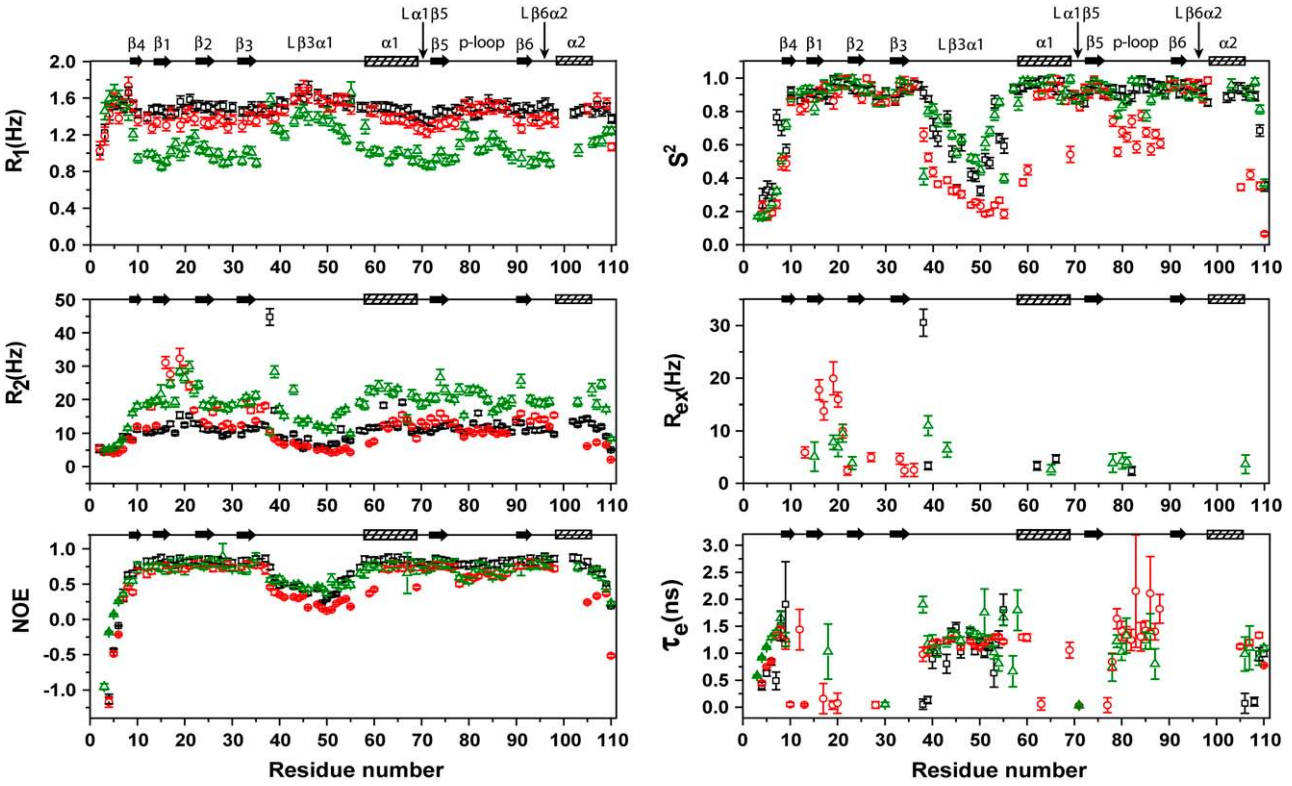

FIGURE 8 Sequence variation of ^{15}N relaxation rates (R_1 and R_2) and ^{15}N-NOEs and the values of the general order parameter, S^2, effective correlation time, τ_e, and the exchange rates, R_{ex}, for G-88W110 (*black square*), V-66W110 (*red circle*), and SNase110 in 2.0 M TMAO (*green triangle*) at 298 K. The secondary structures are labeled at the top of the figure.

order parameters compared to G-88W110. Apparently, the observed backbone dynamic features for V-66W110 must correlate with its less compact structure of higher flexibility in comparison with the structure of G-88W110. The general order parameter values of SNase110 in 2.0 M TMAO spread in a range approximate to the S^2 for G-88W110, except the residues in p-loop which give general S^2 values in a range from 0.77 ± 0.03 to 0.99 ± 0.02 and τ_e values > 0.7 ns (Fig. 8).

The R_{ex} term was required in model-free analysis for some residues of the three fragments. The optimized R_{ex} values for subsets of residues in G-88W110, V-66W110, and SNase110 in 2.0 M TMAO are summarized in Fig. 8. For G-88W110 only a few amide groups display large R_{ex} contributions. Residues L-38 and V-39 with R_{ex} values around 30.58 ± 2.59 and 3.34 ± 0.73 Hz, respectively, occur at the beginning of the disordered loop $L_{\beta3\alpha1}$ of G-88W110, presumably due to the transition from rigid secondary β-sheet structure to a completely flexible $L_{\beta3\alpha1}$ loop. In V-66W110, a contiguous group of residues: T-13, K-16, A-17, D-19, G-20, D-21, Y-27, and T-33 in the segment of β_I-sheet experiences slow conformational exchange motions with $R_{ex} > 3.0$ Hz, indicating higher mobility on the millisecond-microsecond timescale of the β_I-sheet region. Especially, the significant conformational exchange motions ($R_{ex} > 9.0$ Hz) are found for amide groups of residues K-16, A-17, D-19, G-20, and D-21 around β-turn $\tau1$ in the β_I-sheet of V-66W110. For SNase110 in 2.0 M TMAO, the slow exchange motions with $R_{ex} > 3.0$ Hz occur for a number of residues throughout the sequence region I-15–Q-106, among them residues I-15, D-19, G-20, D-21, V-39, and E-43 display large R_{ex} contributions ($R_{ex} > 5.0$ Hz). Residues V-39 and E-43 at the beginning of the disordered loop $L_{\beta3\alpha1}$ in TMAO-stabilized SNase110 show significant R_{ex} contributions ($R_{ex} > 6.0$ Hz), which is a feature common to G-88W110 in this region. Being different from G-88W110, residues D-19, G-20, D-21, and V-23 in the segment around β-turn $\tau1$ of SNase110 in 2.0 M TMAO undergo the slow conformational exchange motions, whereas the R_{ex} contributions and low S^2 values for residues K-78, Q-80, and R-81 in the p-loop suggest some fast internal motions on a subnanosecond-picosecond timescale existing in this region of the fragment. The above described R_{ex} contributions indicate that the higher degree of slow conformational exchange motions occur to residues in the relevant secondary structural regions of V-66W110 and TMAO-stabilized SNase110, but not for G-88W110.

Therefore, the three 110-residue SNase fragments showing different internal motions exhibit different structure rigidity and compactness. G-88W110 adopts a relatively rigid structure having a higher motional restriction for the relevant N-H vectors in secondary structural regions. The less restricted

backbone mobility on a nanosecond-picosecond timescale is observed for V-66W110, which exhibits a less compact structure of higher flexibility. The internal motions of SNase110 in 2.0 M TMAO are more complex, including the relatively high restricted fast internal motions and the contributions from slow conformational exchange which are displayed in G-88W110 and V-66W110, respectively. The fast internal motions dominate in the p-loop of V-66W110 and TMAO-stabilized SNase110. Loop $L_{\beta 3\alpha 1}$ and two terminal regions of all the three fragments are highly flexible.

DISCUSSION

Folding status of the three forms of 110-residue SNase fragment

As has been reported, the native SNase has a main β-barrel hydrophobic core (30) which contains ~40% of the total hydrophobic residues of SNase. Truncating SNase at K-110 disrupts the tertiary hydrophobic interactions in SNase and therefore also disturbs the parking interactions in the β-barrel hydrophobic core of the molecule (30,11). As a result of disrupting the native structure, the retained driving force for folding SNase110 cannot balance with the opposing force from an entropic contribution which is principally responded by conformational freedom (34). This makes SNase110 adopt a conformational ensemble of coexistent partially folded and unfolded states in aqueous solution (10). However, G-88W and V-66W single-point mutations of 110-residue SNase fragment and an effective osmolyte TMAO can raise the unfolding free energies of the fragments (10,35) and facilitate the fragments folding into native-like conformations. The tertiary conformations of G-88W110, V-66W110, and SNase110 in 2.0 M TMAO demonstrate similar native-like β-subdomain structures but exhibit different levels of folding stability, cooperativity, and compactness.

Different folding stabilities of the three 110-residue SNase fragments

Stabilities of G-88W- and V-66W-mutant SNase fragments having different chain lengths were examined previously by GuHCl-induced denaturation experiments. The obtained unfolding free energies revealed a more stable folding of G-88W110 than that of V-66W110 (11). In this study, the folding stabilities of SNase110 and its mutant variants are depicted by the urea-induced denaturation and backbone ^{15}N relaxation data, which describe thermodynamic and structure stabilities, respectively, in the folding of the fragments. G-88W110 has the highest unfolding free energy of the three fragments (Table 2), indicating its high stability to unfolding. The restricted backbone internal motions of the β-barrel and α-helix regions in G-88W110 showing the higher average S^2 value reflect a tightly packed β-barrel hydrophobic core and well-folded α-helices in G-88W110. The β-barrel hydrophobic core of G-88W110 is the most stable of the three fragments, since no explicit conformational exchange motions ($R_{ex} > 3.0$ Hz) can be observed in this structural region. V-66W110 experiences the less restricted fast internal motions and significant slow exchange motions revealed by the low average order parameter S^2 and the large R_{ex} value, respectively. The significant slow conformational exchange motions occur in the β-barrel region of V-66W110, especially at β-turn $\tau 1$ of the β-barrel, which shows a much higher degree of conformational exchange motions. This can be attributed to interconversion between different conformations in the β-turn $\tau 1$ region of the fragment, suggesting a dominant overall conformation with local conformational heterogeneity in V-66W110. The low unfolding free energy of V-66W110 provided by both CD and fluorescence measurements is associated largely with the unstable folding of V-66W110. The unfolding free energy and average order parameter, S^2, estimated from the unfolding transition and backbone relaxation, respectively, for SNase110 in 2.0 M TMAO are close to that for G-88W110 (Table 2 and Fig. 8). However, the R_{ex} contributions displayed in the β-barrel region and at the site around the β-turn $\tau 1$ of TMAO-stabilized SNase110 are supposed to be associated with the lower level of packing in the β-barrel. Apparently, the solvophobic effect of TMAO makes the backbone of SNase110 have restricted fast internal motions, but the β-barrel hydrophobic core remains unstable. The estimated α-helix content (Table 1) of both V-66W110 and SNase110 in 2.0 M TMAO is lower than those of G-88W110, implying the incomplete or less ordered folding of α-helices in V-66W110 and TMAO-stabilized SNase110 compared to that in G-88W110, as displayed by 3D structure determination (Fig. 6).

The above analysis indicates the different folding stabilities of the three 110-residue SNase fragments, which accounts for the different backbone dynamic and urea-unfolding transitions of these fragments. Folding of G-88W110 exhibits a stable structure having a stable β-barrel hydrophobic core. V-66W110 generates an unstable structure having an unstable β-barrel in the tertiary conformation. TMAO-stabilized SNase110, exhibiting relatively high restricted fast internal motions, has an unstable folding of the β-barrel structural region.

Different folding cooperativities of the three 110-residue SNase fragments

In the fully cooperative system undergoing a two-state unfolding, where the ensemble of proteins contains effectively only proteins that are completely folded or highly unfolded, losses of secondary and tertiary structures during unfolding are synchronous (36). The coincidence of fluorescence and CD data from equilibrium denaturation experiments has been taken as an indicator for the two-state folding of a protein. To analyze the cooperative transitions of

the three 110-residue SNase fragments, the equilibrium denaturation transition of full-length SNase was monitored using both fluorescence and CD measurements. Native SNase has a relatively high level of folding cooperativity as shown by superimposability of equilibrium denaturation curves from CD and fluorescence experiments (Fig. 2 *A*) and by the coefficient of cooperativity, *m* (Table 2). The nearly same results of equilibrium denaturation experiments by fluorescence and CD for G-88W110 (Fig. 2 *B*) suggest that the folding of secondary and tertiary structures of G-88W110 is concerted. This implies that G-88W110 can be considered a fully folded 110-residue SNase fragment having native-like ordered secondary structures. In the tertiary structure of native SNase (30), the β-barrel structural region is constructed by two antiparallel β-sheets, namely $\beta_{\rm I}$- and $\beta_{\rm II}$-pleated sheets (Fig. 4 *B*). The 110-residue SNase fragment has a nearly complete sequence of the native β-subdomain of SNase, containing an integrated β-barrel hydrophobic core and two helices α1 and α2. Residue 88 is located at the C-terminal end of the p-loop or the N-terminal of strand β6, which links up strand β5 through the p-loop. The strand β5 is antiparallel to strands β6 and β4 in the $\beta_{\rm II}$-pleated sheet. Obviously, the replacement of glycine by tryptophan at sequence position 88 improves the tertiary interactions in the structural region around residue W-88 and intensifies the hydrophobic packing interactions of residues from strand β6 with the other residues in the β-barrel region. As a result, G-88W110 has a well-packed, native-like β-barrel hydrophobic core and α-helices. The established network of interactions triggered by G-88W mutation should be responsible for the cooperative nature of the equilibrium unfolding transition of G-88W110.

In native SNase, V-66 is one of the residues forming helix α1. A peptide K-70–K-71 links helix α1 with strand β5 of the $\beta_{\rm II}$-pleated sheet. The substitution of tryptophan for valine at sequence position 66 may intensify the hydrophobic interactions of W-66 from helix α1 with hydrophobic residues in the β-barrel region of the protein, generating a native-like β-subdomain structure (Fig. 4 *B*). However, the enhancement of the hydrophobic packing interactions in the β-barrel region by V-66W mutation is not as effective as those by G-88W mutation. The CD and NMR experiments indicate that V-66W mutation can only generate a less ordered and unstable tertiary structure, which exhibits a decreased level of packing in the β-barrel hydrophobic core and incomplete folding of α-helices. Conformation of TMAO- stabilized SNase110 is composed of secondary structural elements that pack together in a manner similar to that seen in G-88W110 (Fig. 4 *B*). Nevertheless, the long-range hydrophobic interactions were disrupted in SNase110 and the effects of TMAO have little if anything to do with the hydrophobic interactions in the protein (35): the remaining hydrophobic interactions in the β-barrel region of TMAO-stabilized SNase110 cannot generate tight packing of side chains in the β-barrel. Thus, the loose packing of the side chains occurs in the β-barrel hydrophobic core, and the secondary α-helix structure is incompletely folded in TMAO-stabilized SNase110 similar to that in V-66W110. The loosely packed β-barrel and incompletely folded α-helical structures of both V-66W110 and TMAO-stabilized SNase110 suggest that both fragments cannot be regarded as fully folded fragments. This may account for the broadening of the unfolding transition obtained by CD measurements for V-66W110 and TMAO-stabilized SNase110 as compared with G-88W110. On the other hand, the CD experiments give approximately the same cooperativity coefficient, *m*, for V-66W110 and TMAO-stabilized SNase110, which is lower than those for G-88W110. Therefore, V-66W110 and TMAO-stabilized SNase110 have a lower level of folding cooperativity than that of G-88W110. The above analysis suggests that the hydrophobic packing interactions in the β-barrel hydrophobic core play an important role in determining the folding cooperativity of the three fragments. Differences in cooperativity seen for the three 110-residue SNase fragments may reflect the different extent of formation of the native-like β-barrel hydrophobic core and α-helix of the fragment.

Different folding compactness of the three 110-residue SNase fragments

Compactness of a protein molecule is highly correlated with the extent of formation of secondary structures in protein and is one of the important properties characterizing the degree of protein folding. The denaturant *m*-value is roughly proportional to the change in solvent exposure during the unfolding transition and thus correlates also with the compactness of a protein (37). Translational diffusion measurement provides directly the apparent molecular size and thus an index of the folding compactness of the three fragments. The 110-residue SNase fragment has a shortage of 39 residues compared to the full-length SNase. Thus, the fully folded G-88W110, giving a molecular size smaller than the size of native SNase (Fig. 7), has a relatively high level of compactness in the structure. However, the low level of compactness is obtained for V-66W110 and TMAO-stabilized SNase110, since the apparent molecular radius of V-66W110 is close to native SNase and the size of TMAO-stabilized SNase110 is larger than those of native SNase (Fig. 7). The *m*-values in Table 2 indicate that the changes in solvent exposure during the unfolding transitions of V-66W110 and TMAO-stabilized SNase110 are smaller than that of G-88W110, implying also less compact structures of both V-66W110 and TMAO-stabilized SNase110. The compactness of G-88W110 can be seen in the packing of residues in the β-barrel hydrophobic core. Compared to the tight packing of side chains of the relevant hydrophobic residues in the β-barrel region of SNase(V8) (Fig. 9), the similar tight packing of the corresponding residues is observed for G-88W110. However, TMAO-stabilized

SNase110 shows the large deviation in the relevant packing (Fig. 9). Therefore, G-88W110 is the most compact of the three 110-residue SNase fragments.

In the β-barrel of native SNase, the three-strand antiparallel β_I-sheet is constructed by the segment T-13–R-35 (Fig. 4 *B*). On the other hand, the three individual segments, H-8–P-11, I-72–F-76, and A-90–Y-93, form the three individual β-strands, β4, β5, and β6, respectively, which form the antiparallel β_{II}-sheet. As was analyzed above, the compactness of the 110-residue SNase fragment is highly correlated with the tightness of the packing of the strands β6 and β5 onto the β_I-sheet in the β-barrel region. Thus, the formation of native-like hydrophobic packing interactions is invoked for tight packing of the β-barrel in the fragment folding. Among the three forms of 110-residue SNase fragment, only G-88W-mutation, increasing the hydrophobicity of the site at residue 88, can consolidate the hydrophobic packing interactions in the β-barrel region, which is verified by a stable, compact structure of G-88W110. The less stable V-66W110 and TMAO-stabilized SNase110 having a low level of compactness may be the consequences of less effective long-range interactions between the residues in the β-barrel region and the residues remote in the sequence of the fragment, which cannot intensify the packing interactions in the β-barrel region. This analysis suggests that the different degree of compactness for the three fragments is determined by the different extent of hydrophobic packing interactions between side chains of the residues in the β-barrel region of G-88W110, V-66W110, and TMAO-stabilized SNase110.

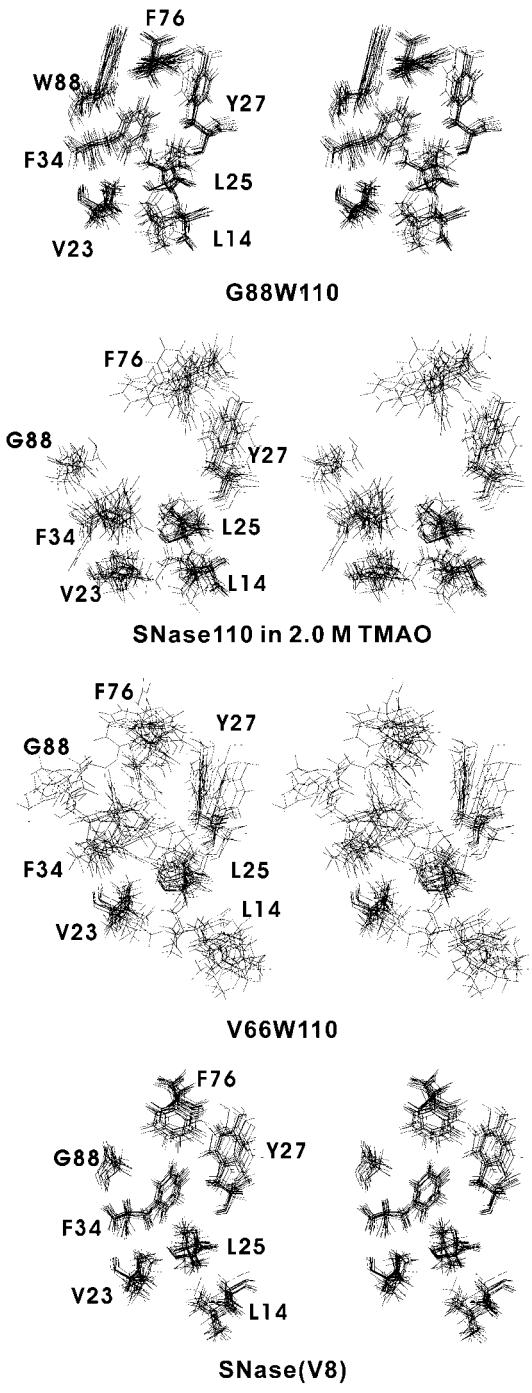

FIGURE 9 Stereo view, showing the packing of the side chains of those hydrophobic residues, which are located mostly in the upper part of the β-barrel region in the tertiary structures of G-88W110, V-66W110, SNase110, and SNase(V8).

Analysis of the conformational states of the three forms of 110-residue SNase fragment reveals a relationship between stability, compactness, and cooperativity in the folding of fragments. The compactness of each conformational state is highly correlated with the extent of formation of a stable, tightly packed β-barrel region. The fragment with higher stability tends to show the higher level of cooperativity in the unfolding transition and higher compactness in structure.

Folding mechanism of the 110-residue SNase fragment

In the partially folded state of SNase110 in aqueous solution (10), the native-like β-turn conformations of the segments around I-18–D-21, Y-27–Q-30, and A-94–K-97, as well as the bend at peptide K-70–K-71 are supposed to be formed transiently based on the similarity of chemical shifts for the dispersed crosspeaks, A-17, G-20, M-26, Y-27, G-29, A-69, K-70, I-72, D-95, and A-96 in the 2D ^{1}H-^{15}N HSQC spectrum of SNase110 to those observed for SNase(V8) (15,16). The preferences for formation of native-like β-turn conformations in these segments of SNase110 are attributed to localized structural propensities that match native structural elements of the same segments in the β-barrel region of native SNase. The localized propensity for turn-like conformations of the sequence regions, I-18–D-21 and Y-27–Q-30, was observed for the N-terminal short fragments of SNase, namely, SNase28, SNase36, and SNase79 containing 1–28, 1–36, and 1–79 residues of SNase, respectively (38,39). In the three-strand antiparallel β_I-sheet spanning the sequence T-13–V-39 of native SNase, the spatial arrangement of

strands β1, β2, and β3 is restricted by the β-turns τ1 (I-18–D-21) and τ2 (Y-27–Q-30) (30). The transiently populated β-sheet-like conformation localized in region T-13–V-39 was observed in SNase79 (39). Therefore, the segments I-18–D-21 and Y-27–Q-30 having the preferences for formation of native-like β-turns can serve as local nucleation sites in the initiation of folding the 110-residue SNase fragments, according to the nucleation mechanism of protein folding (3,40).

The preferential formation of two nascent β-turns in the three 1–110 residues SNase fragments can bring the strands β1, β2, and β3 together to form a native-like antiparallel β_{I}-sheet structure in the segment T-13–V-39 of the fragments. This is evidenced by the G-20I/G-29I double mutation of the 110-residue SNase fragments. The CD, intrinsic fluorescence, and 2D ^{1}H-^{15}N HSQC spectra of G-20I/G-29I double mutant 110-residue SNase fragments (Figs. 1, *B* and *C*, and 3 *D*) reveal dramatic changes in their conformations. The random coil features dominate over the conformations of [G-20I/G-29I]V-66W110 and [G-20I/G-29I]SNase110 in 2.0 M TMAO while the conformation of [G-20I/G-29I] G-88W110 is presented as an ensemble of partially folded and unfolded states. Since the full-length SNase can accommodate isoleucine at positions 20 and 29 (Fig. 8 in Supplementary Materials), the effect of G-20I/G-29I double mutation on fragment folding is not due to the substitution of a branched isoleucine in the turn region of the fragments. Thus, the replacement of glycine at positions 20 and 29 not only disturbs the local intrinsic interactions of the turn segments, but also influences the further formation of the nascent turn structures in the segments I-18–D-21 and Y-27–Q-30, because glycine residues at sequence positions 20 and 29 are required for formation of reverse turns τ1 and τ2 in native SNase. Thereby, the native-like β_{I}-sheet cannot be formed stably in the fragments, causing a serious problem in the packing of the strands β5 and β6 against the β_{I}-sheet, which hinders the double mutant SNase fragments from formation of the β-barrel structural region. In consequence, the tertiary folding of the G-20I/G-29I double mutant 110-residue SNase fragments is largely disrupted. This analysis suggests strongly that the tertiary folding of G-88W110, V-66W110, and SNase110 in 2.0 M TMAO is initiated at the local nucleation sites of I-18–D-21 and Y-27–Q-30.

In the folding of the three 110-residue SNase fragments, the β-barrel structural region behaves as an essential scaffold upon which the α-helical segments of fragment fold, and the packing of strands β5 and β6 against the antiparallel β_{I}-sheet in the β-barrel determines the folding status of the fragments. This was demonstrated in the folding of the 1–79 residues SNase fragment (SNase79). Lacking strand β6 for forming the β-barrel, SNase79 is unable to generate a folded conformation in the presence of TMAO (41). The local packing environment of position 88 in native SNase involves the p-loop and β-barrel structural regions, and that of position 66 involves the helix α1 and β-barrel core. The tightly packed β-barrel in G-88W110 determines a rather compact structure of low flexibility, having well-formed α-helices. The less compact V-66W110 and TMAO-stabilized SNase110 having relatively loosely packed β-barrels generate the incomplete folded α-helices. In light of these, the β-barrel structural region acts more likely as a large nonlocal nucleation site for the further development of structure in the fragment folding.

As is analyzed above, the compactness and stability of structures of the three 110-residue SNase fragments are associated with the stabilities of their β-turn and β-barrel structures, which represent the local and nonlocal nucleation sites for folding the fragments. Thus, a mechanism depicting the folding of G-88W110, V-66W110, and TMAO-stabilized SNase110 can be proposed. The folding of the 110-residue SNase fragment is initiated at the nucleation sites of I-18–D-21 and Y-27–Q-30 and developed by the formation of a nonlocal nucleation site at the β-barrel region, upon which the two α-helices fold. The folding can proceed cooperatively when the local and nonlocal nuclei, namely the β-turn and β-barrel structural regions, are stabilized by the local intrinsic interactions which are consolidated as a result of the formation of native-like long-range interactions. Packing in the local environment of residue 88 has a key importance in formation of the tertiary structure of the 110-residue SNase fragment. This described mechanism for cooperative folding of the 110-residue SNase fragments in vitro may also be applicable to other large SNase fragments and full-length SNase.

CONCLUSIONS

This work describes the folding stability and cooperativity of the three forms of 110-residue SNase fragment. The G-88W and V-66W single mutation and solvophobic effect of TMAO can drive 110-residue SNase fragment folding into a native-like conformation. The tertiary conformations, unfolding free energies, and internal motions of G-88W110, V-66W110, and SNase110 in 2.0 M TMAO and their G-20I/G-29I double mutant variants depict the folding features of the 110-residue SNase fragments. The tertiary folding of G-88W110 produces an ordered conformation, representing a native-like β-subdomain, which is the most stable of the three fragments. V-66W-mutant and the TMAO-stabilized 110-residue SNase fragments generate less ordered and unstable tertiary structures compared to G-88W110. The hydrophobic core packing in the β-barrel region between β_{I}- and β_{II}-sheets has a profound effect on native-like folding of the fragment, and the native-like β-barrel structural region acts as a nonlocal nucleus for folding the fragment. The tertiary folding of G-88W110, V-66W110, and SNase110 in 2.0 M TMAO is initiated by formation of the local nucleation sites at two β-turn regions, I-18–D-21 and Y-27–Q-30, and developed by the formation of a nonlocal nucleation site at the β-barrel region. The folding of the fragment proceeds cooperatively when the local intrinsic interactions are consolidated by the

formation of the tertiary long-range interactions in the fragment. The mechanism applied in the folding of the 110-residue SNase fragments may also be applicable to other large SNase fragments and full-length SNase.

Coordinates

The atomic coordinates of G-88W110, V-66W110, and SNase110 in 2.0 M TMAO have been deposited in the Protein Data Bank (accession code 1RKN, 2F3V, and 2F3W, respectively) and chemical shifts of G-88W110, V-66W110, and SNase110 in 2.0 M TMAO have been deposited in BioMagResBank along with associated NMR parameters (accession number 5536, 6907, and 6908, respectively).

SUPPLEMENTARY MATERIAL

An online supplement to this article can be found by visiting BJ Online at http://www.biophysj.org.

This research was supported by the National Natural Science Foundation of China (NNSFC) 30570375 and partly by NNSFC 39823001.

REFERENCES

1. Fersht, A. R., and V. Daggett. 2002. Protein folding and unfolding at atomic resolution. *Cell.* 108:573–582.
2. Fersht, A. R. 1997. Nucleation mechanisms in protein folding. *Curr. Opin. Struct. Biol.* 7:3–9.
3. Brooks 3rd, C. L., M. Gruebele, J. N. Onuchic, and P. G. Wolynes. 1998. Chemical physics of protein folding. *Proc. Natl. Acad. Sci. USA.* 95:11037–11038.
4. Ye, K., G. Jing, and J. Wang. 2000. Interactions between subdomains in the partially folded state of staphylococcal nuclease. *Biochim. Biophys. Acta.* 1479:123–134.
5. Alexandrescu, A. T., A. G. Gittis, C. Abeygunawardana, and D. Shortle. 1995. NMR structure of a stable ''OB-fold'' sub-domain isolated from staphylococcal nuclease. *J. Mol. Biol.* 250:134–143.
6. Wang, Y., and D. Shortle. 1995. The equilibrium folding pathway of staphylococcal nuclease: identification of the most stable chain-chain interactions by NMR and CD spectroscopy. *Biochemistry.* 34:15895–15905.
7. Ermacora, M. R., D. W. Ledman, and R. O. Fox. 1996. Mapping the structure of a non-native state of staphylococcal nuclease. *Nat. Struct. Biol.* 3:59–66.
8. Eftink, M. R., R. Ionescu, G. D. Ramsay, C. Wong, J. Wu, and A. H. Maki. 1996. Termodynamics of the unfolding and spectroscopic properties of the V66W mutant of staphylococcal nuclease and its 1–136 fragment. *Biochemistry.* 35:8084–8094.
9. Hirano, S., K. Mihara, Y. Yamazaki, H. Kamikubo, Y. Imamoto, and M. Kataoka. 2002. Role of C-terminal region of staphylococcal nuclease for foldability, stability, and activity. *Proteins.* 49:255–265.
10. Feng, Y., D. Liu, and J. Wang. 2003. Native-like partially folded conformations and folding process revealed in the N-terminal large fragments of staphylococcal nuclease: a study by NMR spectroscopy. *J. Mol. Biol.* 330:821–837.
11. Ye, K., G. Jing, and J. Wang. 2000. Interactions between subdomains in the partially folded state of staphylococcal nuclease. *Biochim. Biophys. Acta.* 1479:123–134.
12. Hemsley, A., N. Arnheim, M. D. Toney, G. Cortopassi, and D. J. Galas. 1989. A simple method for site-directed mutagenesis using the polymerase chain reaction. *Nucleic Acids Res.* 17:6545–6551.
13. Pace, C. N. 1986. Determination and analysis of urea and guanidine hydrochloride denaturation curves. *Methods Enzymol.* 131:266–280.
14. Santoro, M. M., and D. W. Bolen. 1988. Unfolding free energy changes determined by the linear extrapolation method. 1. Unfolding of phenylmethanesulfonyl alpha-chymotrypsin using different denaturants. *Biochemistry.* 27:8063–8068.
15. Wang, J., E. S. Mooberry, W. F. Walkenhorst, and J. L. Markley. 1992. Solution studies of staphylococcal nuclease H124L. 1. Backbone ^{1}H and ^{15}N resonances and secondary structure of the unligated enzyme as identified by three-dimensional NMR spectroscopy. *Biochemistry.* 31:911–920.
16. Wang, J., A. P. Hinck, S. N. Loh, D. M. LeMaster, and J. L. Markley. 1992. Solution studies of staphylococcal nuclease H124L. 2. ^{1}H, ^{13}C, and ^{15}N chemical shift assignments for the unligated enzyme and analysis of chemical shift changes that accompany formation of the nuclease-thymidine 3′,5′-bisphosphate-calcium ternary complex. *Biochemistry.* 31:921–936.
17. Jones, J. A., D. K. Wilkins, and L. J. Smith. 1997. Characterization of protein unfolding by NMR diffusion measurements. *J. Biomol. NMR.* 10:199–203.
18. Zhu, G., and A. Bax. 1992. Improved linear prediction of damped NMR signals using modified forward back linear prediction. *J. Magn. Reson.* 100:202–207.
19. Cavanaugh, J., W. J. Fairbrother, A. G. Palmer, and N. J. Skelton. 1996. Protein NMR Spectroscopy. Academic Press, San Diego, CA.
20. Farrow, N. A., R. Muhandiram, A. U. Singer, S. M. Pascal, C. M. Kay, G. Gish, S. E. Shoelson, T. Pawson, J. D. Forman-Kay, and L. E. Kay. 1994. Backbone dynamics of a free and phosphopeptide-complexed Src homology 2 domain studied by ^{15}N NMR relaxation. *Biochemistry.* 33:5984–6003.
21. Cornilescu, G., F. Delaglio, and A. Bax. 1999. Protein backbone angle restraints from searching a database for chemical shift and sequence homology. *J. Biomol. NMR.* 13:289–302.
22. Brunger, A. T., P. D. Adams, G. M. Clore, W. L. DeLano, P. Gros, R. W. Grosse-Kunstleve, J. S. Jiang, J. Kuszewski, M. Nilges, N. S. Pannu, R. J. Read, L. M. Rice, T. Simonson, and G. L. Warren. 1998. Crystallography & NMR system: a new software suite for macromolecular structure determination. *Acta Crystallogr. D Biol. Crystallogr.* 54:905–921.
23. Lipari, G., and A. Szabo. 1982. Model-free approach to the interpretation of nuclear magnetic resonance relaxation in macromolecules. 1. Theory and range of validity. *J. Am. Chem. Soc.* 104:4546–4559.
24. Lipari, G., and A. Szabo. 1982. Model-free approach to the interpretation of nuclear magnetic resonance relaxation in macromolecules. 2. Analysis of experimental results. *J. Am. Chem. Soc.* 104:4559–4570.
25. Cole, R., and J. P. Loria. 2003. FAST-Modelfree: a program for rapid automated analysis of solution NMR spin-relaxation data. *J. Biomol. NMR.* 10:203–213.
26. Kay, L. E., D. A. Torchia, and A. Bax. 1989. Backbone dynamics of proteins as studied by ^{15}N inverse-detected heteronuclear NMR-spectroscopy-application to staphylococcal nuclease. *Biochemistry.* 28: 8972–8979.
27. Dosset, P., J. C. Hus, M. Blackledge, and D. Marion. 2000. Efficient analysis of macromolecular rotational diffusion from heteronuclear relaxation data. *J. Biomol. NMR.* 16:23–28.
28. Mandel, A. M., M. Akke, and A. G. Palmer. 1995. Backbone dynamics of Escherichia coli ribonuclease HI: correlations with structure and function in an active enzyme. *J. Mol. Biol.* 246:144–163.
29. Schwarzinger, S., G. J. Kroon, T. R. Foss, J. Chung, P. E. Wright, and H. J. Dyson. 2001. Sequence-dependent correction of random coil NMR chemical shifts. *J. Am. Chem. Soc.* 123:2970–2978.
30. Wang, J., D. M. Truckses, F. Abildgaard, Z. Dzakula, Z. Zolnai, and J. L. Markley. 1997. Solution structures of staphylococcal nuclease from multidimensional, multinuclear NMR: nuclease-H124L and its ternary complex with Ca^{2+} and thymidine-3′,5′-bisphosphate. *J. Biomol. NMR.* 10:143–164.

31. Laskowski, R. A., J. A. Rullmannn, M. W. MacArthur, R. Kaptein, and J. M. Thornton. 1996. AQUA and PROCHECK-NMR: programs for checking the quality of protein structures solved by NMR. *J. Biomol. NMR.* 8:477–486.

32. Koradi, R., M. Billeter, and K. Wuthrich. 1996. MOLMOL: a program for display and analysis of macromolecular structures. *J. Mol. Graph.* 14:51–55.

33. Flanagan, J. M., M. Kataoka, T. Fujisawa, and D. M. Engelman. 1993. Mutations can cause large changes in the conformation of a denatured protein. *Biochemistry.* 32:10359–10370.

34. Dill, K. A. 1990. Dominant forces in protein folding. *Biochemistry.* 29:7133–7155.

35. Baskakov, I., and D. W. Bolen. 1998. Forcing thermodynamically unfolded proteins to fold. *J. Biol. Chem.* 273:4831–4834.

36. Batey, S., L. G. Randles, A. Annette Steward, and J. Clarke. 2005. Cooperative folding in a multi-domain protein. *J. Mol. Biol.* 349:1045–1059.

37. Parker, M. J., J. Spencer, and A. R. Clarke. 1995. An integrated kinetic analysis of intermediates and transition states in protein folding reactions. *J. Mol. Biol.* 253:771–786.

38. Dai, J., X. Wang, Y. Feng, G. Fan, and J. Wang. 2004. Searching for folding initiation sites of staphylococcal nuclease: a study of N-terminal short fragments. *Biopolymers.* 75:229–241.

39. Wang, X., Y. Tong, and J. Wang. 2005. *Cis*/*trans* heterogeneity of Gln30-Pro31 peptide bond determines whether a 79-residue fragment of staphylococcal nuclease self-associates. *Biochem. Biophys. Res. Commun.* 329:495–501.

40. Itzhaki, L. S., D. E. Otzen, and A. R. Fersht. 1995. The structure of the transition state for folding of chymotrypsin inhibitor 2 analysed by protein engineering methods: evidence for a nucleation-condensation mechanism for protein folding. *J. Mol. Biol.* 254:260–288.

41. Wang, X., M. Wang, Y. Tong, L. Shan, and J. Wang. 2006. Probing the folding capacity and residual structures in 1–79 residues fragment of staphylococcal nuclease by biophysical and NMR methods. *Biochimie* 88:1343–1355.